RL-TR-96-139
Final Technical Report
July 1996

SUBWAVELENGTH-STRUCTURED SURFACES FOR OPTICAL INTERCONNECTS

Cornell University

Frederick T. Chen, J. Greg Couillard,
and Harold G. Craighead
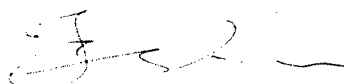
DTIC QUALITY INSPECTED 4

19961008 010

Rome Laboratory
Air Force Materiel Command
Rome, New York

This report has been reviewed by the Rome Laboratory Public Affairs Office (PA) and is releasable to the National Technical Information Service (NTIS). At NTIS, it will be releasable to the general public, including foreign nations.
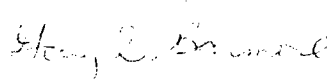
RL-TR- 96-139 has been reviewed and is approved for publication.

APPROVED:

FRANZ HAAS
Project Engineer

FOR THE COMMANDER:

GARY D. BARMORE, Major, USAF
Deputy Director
Surveillance & Photonics

REPORT DOCUMENTATION PAGE

1. AGENCY USE ONLY (Leave Blank)	2. REPORT DATE July 1996	3. REPORT TYPE AND DATES COVERED Final Feb 94 – Aug 95

4. TITLE AND SUBTITLE

SUBWAVELENGTH-STRUCTURED SURFACES FOR OPTICAL INTERCONNECTS

6. AUTHOR(S)

Frederick T. Chen, J. Greg Couillard, and Harold G. Craighead

5. FUNDING NUMBERS

C – F30602-94-C-0028
PE – 62702F
PR – 4600
TA – P3
WU – PV

7. PERFORMING ORGANIZATION NAME(S) AND ADDRESS(ES)

Cornell University
Office of Sponsored Programs
120 Day Hall
Ithaca NY 14853-2801

8. PERFORMING ORGANIZATION REPORT NUMBER

N/A

9. SPONSORING/MONITORING AGENCY NAME(S) AND ADDRESS(ES)

Rome Laboratory /OCPA
25 Electronic Pkwy
Rome NY 13441-4515

10. SPONSORING/MONITORING AGENCY REPORT NUMBER

RL-TR-96-139

11. SUPPLEMENTARY NOTES

Rome Laboratory Project Engineer: Franz Haas/OCPA/(315)330-2131

12a. DISTRIBUTION/AVAILABILITY STATEMENT

Approved for public release; distribution unlimited.

12b. DISTRIBUTION CODE

13. ABSTRACT (Maximum 200 words)

The fabrication of sub-wavelength structures has been used to develop efficient diffractive optical elements with a single mask/etch step as well as optically absorptive areas. By the controlled removal of a substrate material in sub-wavelength units, the effective refractive index of the substrate material can be varied from the original index to that of air or other fill material. Diffractive elements can be fabricated by varying the substrate refractive index in a diffractive pattern. A linear grating and a spherical diffractive lens were fabricated in fused quartz for use at the 632.8nm wavelength. A technique for fabricating sub-micron structures in silicon was also developed. The micro-structures have reflectances of as low as 0.05% and less than 0.5% across the visible spectrum. These structures can be used as antireflection coatings in silicon-based optoelectronic systems.

14. SUBJECT TERMS

Optical interconnects, Diffractive Optics, Antireflection Coating

15. NUMBER OF PAGES
40

16. PRICE CODE

17. SECURITY CLASSIFICATION OF REPORT UNCLASSIFIED	18. SECURITY CLASSIFICATION OF THIS PAGE UNCLASSIFIED	19. SECURITY CLASSIFICATION OF ABSTRACT UNCLASSIFIED	20. LIMITATION OF ABSTRACT UL

Final Report

Subwavelength-Structured Surfaces for Optical Interconnects

Frederick T. Chen, J. Greg Couillard, Harold G. Craighead

School of Applied and Engineering Physics, Ithaca, NY 14853-2501

Final Contract report:

Subwavelength-Structured Surfaces for Optical Interconnects

Frederick T. Chen, J. Greg Couillard, Harold G. Craighead

School of Applied and Engineering Physics, Ithaca, NY 14853-2501

We demonstrate that subwavelength-structured surfaces may find potential applications in optical interconnect networks. Square arrays of pillars and holes have been fabricated in fused quartz substrates as components of diffractive optical elements operating at 632.8 nm. "Black silicon", i.e., irregular arrays of subwavelength features in silicon produced by random masking and etching, has been shown to enhance absorption in the visible spectrum. Ths different aspects fo this work are described in sections I, II and III.

Introduction

The underlying concept behind a subwavelength-structured surface requires visualizing a diffraction grating. For a given period d, and normal incidence, the diffraction orders are given by the grating equation $d \sin q_m = ml$. As d gets smaller, the spacings between angles increases, and the +/- 1st orders approach 90°. Once d is smaller than a wavelength these orders have "disappeared over the horizon." Essentially all energy is carried away by the reflected and transmitted zeroth orders. For a lossy substrate, energy that does not go into the reflected zeroth order (the specular reflection) is absorbed. Thus, when the spacing between features is less than a wavelength, there is no scattering from the array and the entire array appears homogeneous. Alternatively, one may think of the features as being smaller than the resolution of incident light at a given wavelength l.

Motivation

The motivation behind the present work is to simplify the fabrication of components for free-space optical interconnection networks. Routing elements would include lenses and phase gratings, which may be fabricated using subwavelength structures. The interconnection occurs because of artificial index modulation in the surface of the element, brought about by suitably modulating the feature sizes. The use of artificial index modulation as an alternative to surface relief modulation is motivated by the difficulty of producing precisely sloped profiles by lithography and etching (see for example, Daschner et. al., Applied Optics **34**, 2534 (1995)) as well as the accumulated errors from the multiple mask scheme of traditional binary optics (see Shank et. al., JVST B **12**, 3643 (1995)). Details of this phase of our work are given in two of our publications, Optics Letters **20**, 121 (1995) and Optics Letters **21**, 177 (1996), both by Chen and Craighead.

In addition to routers, subwavelength structures would be useful components of detectors. A detector with a textured surface, e.g., black silicon, would have an enhanced efficiency over one with an unpatterned surface. Details are given in an unpublished report by Couillard and Craighead.

I. Diffractive phase elements based on two-dimensional artificial dielectrics

Frederick T. Chen and H. G. Craighead

We have designed, fabricated and tested a blazed artificial dielectric transmission grating in fused quartz for use at 633 nm wavelength. By locally varying the index using fabricated two-dimensional arrays of dielectric cylinders, a desired phase modulation can be achieved to produce a diffractive phase element in one processing step. The effective index depends on the fill fraction of the cylinders.

There has long been an interest in tailoring the dielectric properties of materials for desired optical applications. It has been discussed in the literature[1-4] that an array of dielectric objects behaves as a homogeneous dielectric medium if the period of the array is small enough to exclude all propagating diffraction orders except the zeroth order. Artificial dielectrics hold great promise for the fabrication of phase-only diffractive elements, since they can be produced using one straightforward lithography step followed by etching or replicated from a master produced this way. This avoids the need for alignment between multiple lithography-and-etch steps or carefully tailoring continuous resist or substrate surface profiles. Varied-index diffractive elements and antireflection gratings based on artificial dielectrics have been proposed by many authors.[1-4] In this Letter, a simple procedure for designing artificial dielectrics using two-dimensional subwavelength gratings is discussed. In addition, a blazed artificial dielectric grating designed by this procedure and fabricated in fused quartz for use with a HeNe laser (1 = 633 nm) is demonstrated for the first time.

In order to be able to readily design and fabricate artificial dielectric elements, one must be able to relate the effective index to the grating profile in a simple way. By solving Maxwell's equations with the relevant boundary conditions, the effective indices of 1D and 2D subwavelength gratings have been obtained numerically by many authors.[1,4,5] Alternatively, the use of effective medium theory generally yields a good approximation if

the period/wavelength ratio is sufficiently small.[1] For 1D gratings, the theory gives simple expressions for the ordinary and extraordinary indices as follows:

$$n_{TE}^2 = f_1 n_1^2 + f_2 n_2^2 \tag{1}$$

$$n_{TM}^{-2} = f_1 n_1^{-2} + f_2 n_2^{-2} \tag{2}$$

where f_1 is the fill factor for medium 1 and $f_2 = 1-f_1$ is the fill factor for medium 2.[6] The different indices for the two polarization states indicate that 1D subwavelength gratings have form birefringence. Equations (2) and (3) are well known results and have been frequently compared with rigorous calculations.[1-4]

The index in the direction normal to the grating vectors of a 2D subwavelength grating is given in effective medium theory by

$$n_z = \left(\left(1 - f_x f_y\right) n_1^2 + f_x f_y n_2^2 \right)^{1/2}, \tag{3}$$

where f_x and f_y are the fill factors of medium 2 in the x- and y-directions respectively. It has been noted that there are no simple closed-form zero-order expressions for the transverse principal effective indices of a 2D subwavelength grating.[1,5] On the other hand, the indices can be bounded approximately using simple expressions derived from effective medium theory.[7] For simplicity, we will consider rectangular cylindrical geometries only. To set the upper bound, the 2D rectangular grating is viewed as a 1D grating consisting of strips lined up perpendicular to the electric field. Each strip in turn can be thought of as a section of a 1D grating with ridges parallel to the electric field. The effective index of each strip is calculated using (1). These strip indices are then used to calculate the overall effective index using (2). This effective index is an upper bound which is exact in the static case and is given by

$$n_{upp,x} = \left(\frac{1-f_x}{n_1^2} + \frac{f_x}{f_y n_2^2 + (1-f_y) n_1^2} \right)^{-1/2}. \tag{4}$$

To obtain the lower bound, the 2D grating is viewed as a 1D grating consisting of strips parallel to the electric field. The effective index of each strip is now found using (2), and the overall effective index, representing the lower bound, using (1), giving

$$n_{low,x} = \left((1 - f_y) n_1{}^2 + \frac{f_y}{f_x / n_2{}^2 + (1 - f_x) / n_1{}^2} \right)^{1/2}. \tag{5}$$

The effective index bounds in the y-direction are obtained by interchanging the x and y subscripts. At all times, the bounds lie between the indices of the two components of the artificial dielectric. For an artificial dielectric consisting of two materials with similar dielectric constants, the bounds are usually very narrow, e.g., < 2% for fused quartz and air. Thus, in the case of fused quartz and air, the index is virtually fixed with considerable accuracy. In his important paper, however, Rytov derived corrections to (1) and (2), assuming normal incidence, which took into account the magnitude of the period/wavelength ratio d/l as well as the dielectric constants of the two constituents.[8] Using two materials with similar dielectric constants relaxes the requirement that d/l<<1 for the static approach to be a good approximation, at normal incidence. For a 2D 400 nm period symmetric grating in a fused quartz substrate at a wavelength of 633 nm, the effective indices, corrected to second order in d/l, are on the average increased by at most ~3%.

Figures 1 and 2 show the lower and upper bounds for a square array of square quartz pillars and square holes in quartz, respectively. The square symmetry guarantees that there is no polarization sensitivity for light propagating along the axis of the pillars or holes. This is a requirement for designing any diffractive element for normal incident light of unspecified polarization, e.g., a Fresnel lens. If the grating profile does not possess square symmetry, a different effective index for each polarization direction is to be expected. This may be useful for designing polarization beamsplitters and birefringence compensators. It should be noted that the use of quartz pillars allows easier access to indices near n=1. Likewise, the use of holes allows easier access to indices near that of quartz, n=1.46.

Accordingly, a first order artificial dielectric transmission grating with a period of 24 μm has been designed for normally incident light at a wavelength of 633 nm and

fabricated in fused quartz. A 70 nm layer of PMMA was spin coated onto a fused quartz substrate coated with a 100 nm layer of thermally evaporated aluminum. Six roughly equally spaced effective indices, ranging from 1.07 to 1.46, were used to produce the desired blazing effect. The indices were achieved by using a 20 kV 70-nm diameter electron beam to write square quartz pillars and holes of varying size according to Figures 1 and 2, respectively. Both feature size data and dose needed to be simultaneously adjusted to obtain sizes as close to desired as possible. The effective index of each strip is generated from a 2D square array of square pillars or holes with a period of 400 nm. As mentioned earlier, at normal incidence, this period is sufficiently small to guarantee that only the zeroth transmitted and reflected orders propagate, and for the static results to be reasonably accurate. This period is also significantly large enough, compared to the beam size, to allow large index modulation. Pattern transfer into the fused quartz is accomplished by two reactive ion etching steps. The first step transfers the pattern anisotropically from the resist to the aluminum mask, using a $Cl_2/BCl_3/CH_4$ plasma. The second etch transfers the pattern from the mask to the quartz substrate. The necessary etch depth into the substrate for a first order transmission grating is $h = \lambda/(n-1) = 1.38 \ \mu m$. Aspect ratios of almost 10:1 are easily accomplished since the aluminum mask does not erode significantly as the quartz substrate is being etched. This was accomplished at low ion energies (~150 V) with a magnetically confined CHF_3 plasma resulting in enhanced ion densities.

A scanning electron micrograph of one period of the grating is shown in Figure 3. The optical performance is displayed in Figure 4. The grating showed a first order diffraction efficiency of 55% for both TE and TM polarizations. In fact, both polarizations showed identical efficiencies, to within 0.5%, in all the orders that were measured (-7 to 7). The maximum theoretical first order efficiency for a 6-level diffractive optical element is 88%, taking into consideration Fresnel losses. The discrepancy is due to errors in obtaining the correct phase modulation. Performance may be improved by properly fine-tuned exposure. At present it is difficult to correctly achieve the desired feature sizes and

shapes, due to proximity effects. However, the dependence of effective index on feature shape is not expected to be significant, as long as the relative volume fractions remain the same.[9] Even with accurately defined effective indices, however, there is yet another problem: RIE lag.[10] Smaller holes are not etched as deep as larger holes, thus reducing the actual phase shift below the desired value.

The simple 2D design procedure outlined in this Letter facilitates the design of more sophisticated artificial dielectric diffractive optical elements. A slow variation of fill factor across a period of the deflection grating would produce an effective continuous index gradient. Creating a radial index variation would result in a diffractive lens. By employing pyramidal gratings, antireflection behavior can be achieved and incorporated into the diffractive phase element.[1,2] Finally, birefringence may be adjusted by means of the extra duty cycle.

References - section I

1. D. H. Raguin and G. M. Morris, Appl. Opt. 32, 1154 (1993).

2. R. C. Enger and S. K. Case, Appl. Opt. 22, 3220 (1983).

3. T. K. Gaylord, W. E. Baird, and M. G. Moharam, Appl. Opt. 25, 4562 (1986).

4. S. Babin, H. Haidner, P. Kipfer, J. T. Sheridan, W. Stork, and N. Streibl, SPIE 1751, 202 (1992).

5. E. B. Grann, M. G. Moharam, and D. A. Pommet, JOSA 11, 2695 (1994).

6. M. Born and E. Wolf, *Principles of Optics*, 6th ed., Pergamon Press, 1980, p. 706.

7. J. L. Jackson and S. R. Coriell, Journ. of Appl. Phys. 39, 2349 (1968).

8. S. M. Rytov, Sov. Phys. JETP, 2, 466 (1956).

9. S. R. Coriell and J. L. Jackson, Journ. of Appl. Phys. 39, 4733 (1968).

10. O. Joubert , G. S. Oehrlein, and Y. Zhang, JVST A 12, 658 (1994).

Figure captions - section I

Figure 1. Bounds on the effective index derived from a square subwavelength array of square quartz pillars as a function of the pillar size/period ratio.

Figure 2. Bounds on the effective index derived from a square subwavelength array of square holes in quartz as a function of the pillar size/period ratio.

Figure 3. A scanning electron micrograph of one period of the artificial dielectric grating.

Figure 4. Diffraction efficiencies for both polarizations for -7th to 7th orders.
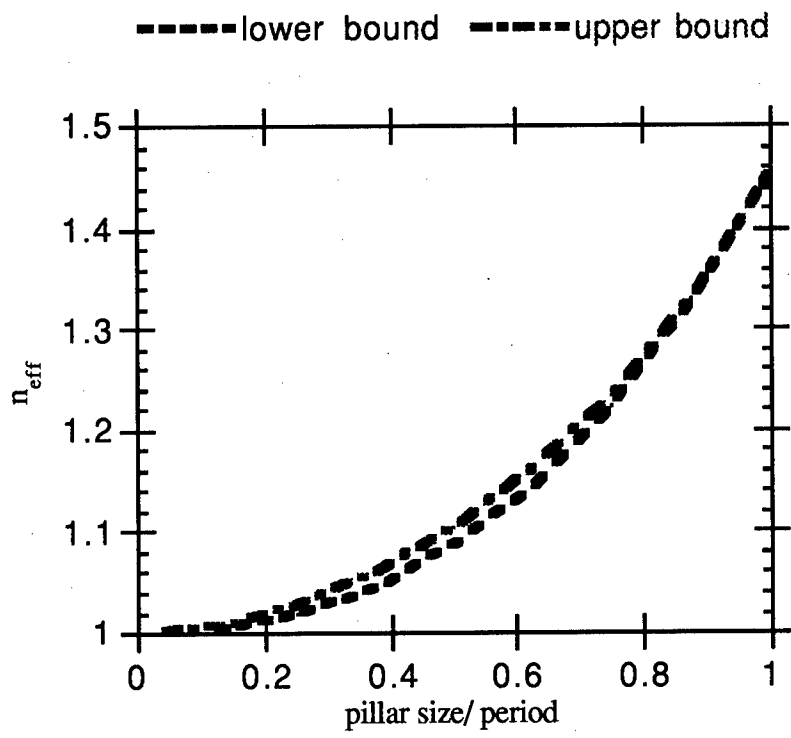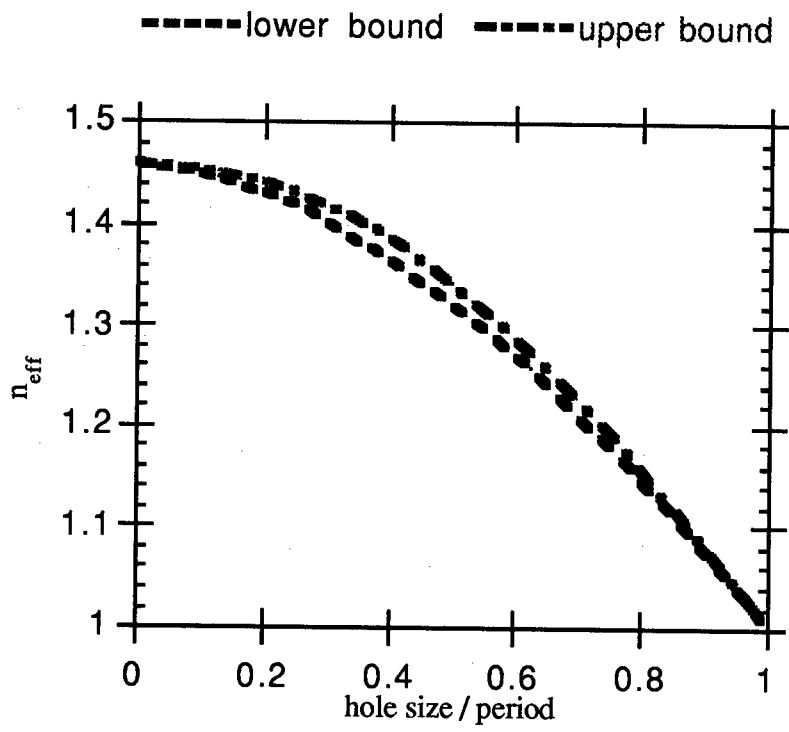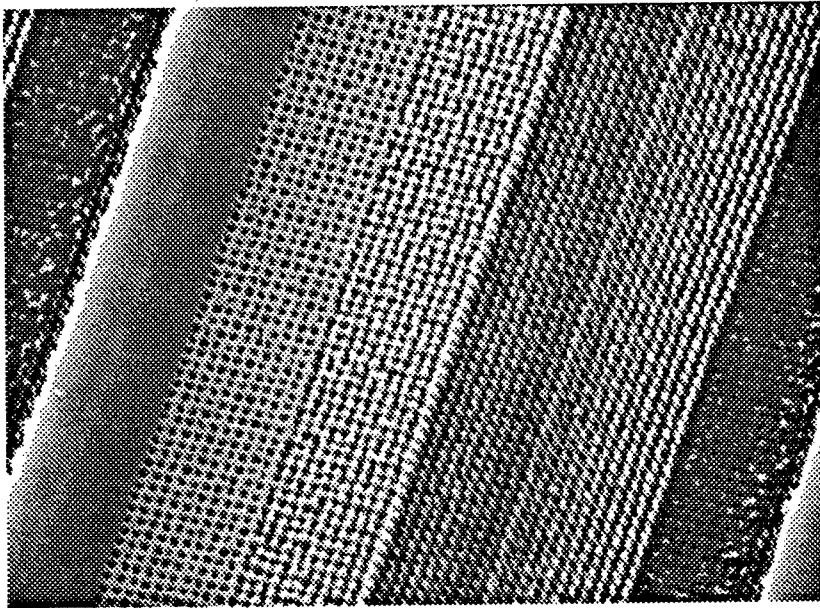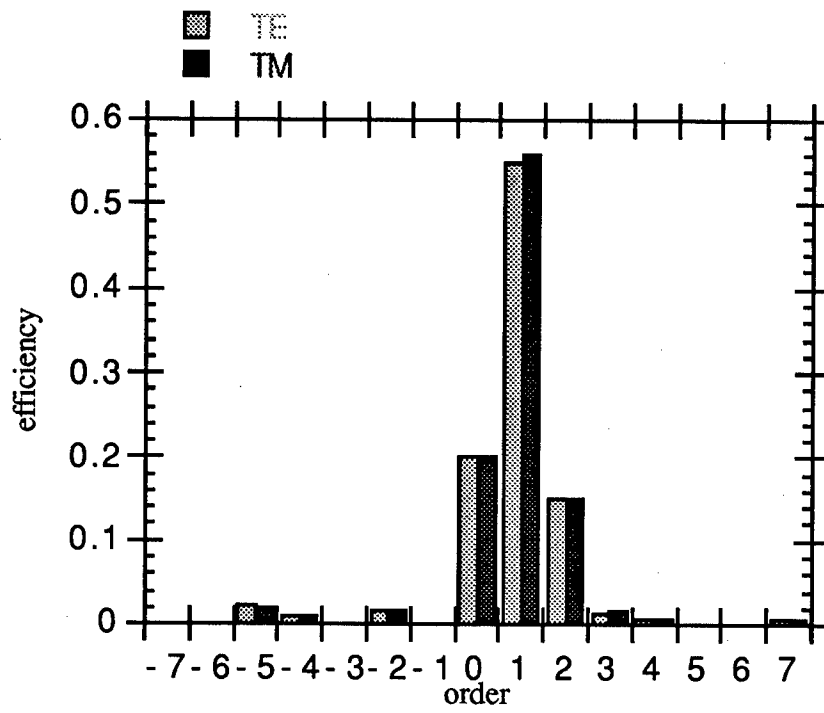
Figure Ī -1

Figure I -2

10 μm

Figure I - 3

Figure I - 4

II. Diffractive lens fabricated with mostly-zeroth-order gratings

Frederick T. Chen and Harold G. Craighead

We demonstrate a spherical diffractive lens fabricated in fused quartz for use at the 632.8 nm wavelength. The lens is constructed using a modulated two-dimensional binary grating with a high transmitted zeroth order efficiency. Rigorous eigenmode analysis is used to correlate the desired phase modulation with the fill factor. Fabrication requires only one lithography step. Using the lens, we were able to image a focal spot with a diffraction-limited spot size (FWHM).

Carefully arranged subwavelength microstructures constitute artificial dielectric optical components. This was first demonstrated using microwaves.[1] The concept was applied to diffractive optical elements independently by Stork et. al. and Farn.[2,3] Recently, we have demonstrated a transmissive blazed grating fabricated in fused quartz at a visible wavelength (l=632.8 nm) that was designed using an approximate effective medium theory for two-dimensional zero-order dielectric gratings.[4] Kipfer et. al. have demonstrated diffractive spherical mirrors based on a similar principle at the 10.6 μm wavelength.[5] In previous work, the periods of the gratings to be modulated were chosen so that only one transmitted and one reflected order were propagating. For low index dielectric substrates, this ensures a high transmitted zeroth order efficiency. As we show in this Letter, however, larger periods allowing more orders to propagate can be used, as long as the transmitted zeroth order efficiency is sufficiently high. Such gratings may be called mostly-zeroth-order gratings (MZOGs). The main advantage of using larger periods is that fabrication is easier, at the cost of somewhat lower efficiencies. In this Letter, we demonstrate what we believe to be the first diffractive lens designed using mostly-zeroth-order gratings and fabricated in a fused quartz substrate for operation at the 632.8 nm wavelength.

The basic strategy for designing transmissive binary diffractive optical elements with high efficiency has been described.[2-4,6] The function of the element is determined by

the macrostructure, i.e., the large-scale phase profile. For paraxial applications, scalar theory is adequate for finding the optimum phase profile for operation of the element. The phase profile is not generated directly by the surface relief but by the local microstructure, which consists of a high-spatial-frequency dielectric grating that allows most of the incident light to pass into the transmitted zeroth order. The phase of the transmitted zeroth order light is determined by the fill factor of the grating, as well as the period/wavelength ratio d/l and the grating depth h. Hence, by modulating the fill factor while keeping the period and depth fixed, one obtains arbitrary phase modulation over the entire aperture of the diffractive element. The high-spatial-frequency grating is effectively homogenized into an artificial dielectric layer. In contrast to the macrostructure, a rigorous vectorial approach is required for describing the high-spatial-frequency grating microstructure. Rigorous eigenmode theory[6,7] is a natural and efficient method for analyzing surface-relief dielectric gratings. Noponen and Turunen[6] have suggested the use of high-spatial-frequency lamellar dielectric gratings with periods as large as 0.8l. If two-dimensional symmetric gratings are used, calculations based on rigorous eigenmode analysis[7] show that at normal incidence, transmitted zeroth order efficiencies of $\geq 80\%$ may be achieved for all fill factors with periods as large as 1.1l for grating depths allowing sufficient phase modulation ($f_{max} \sim 3\pi/2$-2π). Surprisingly, this is not true for TE-polarized light normally incident onto a lamellar grating. Moreover, at normal incidence, a symmetric 2D grating exhibits no polarization sensitivity.

For the purpose of demonstrating the basic principle, we modeled a square array of square pillars 1.032 um tall with a period of 700 nm. Normal incidence from a quartz substrate (n=1.46) to air was assumed. 13 Rayleigh orders along each axis were retained in our calculations. This height was chosen to accomodate a phase range of 0 to $3\pi/2$. According to scalar theory, this phase range yields a first-order diffraction efficiency of 81% for a four-level staircase phase profile.[8] By using pillars, reactive ion etching lag effects can be avoided during the fabrication process, since reactant and product transport

are not hindered significantly.[9,10] In Figure 1, we plot the efficiency and phase of the transmitted zeroth order as a function of pillar width. Only the component polarized parallel to that of the incident light is plotted. The calculated amount of depolarization in the zeroth order actually never exceeds several percent. For volume fractions sufficiently near zero or unity, one may expect near-homogeneous behavior (less scattering). For pillar widths above 350 nm and below 600 nm, there is increased scattering into higher diffraction orders, resulting in the dip in the transmitted zeroth order efficiency.

Using the data of Fig. 1 as a lookup table, we have designed and fabricated a diffractive lens in fused quartz for focusing normally incident 632.8 nm light. The lens had a square aperture 1 mm on a side, and a focal length of 2 cm. A fused quartz substrate was first coated with 100 nm of thermally evaporated aluminum. A 70-nm-thick layer of poly(methyl-methacrylate) (PMMA) was then spin coated onto the aluminum layer. The pattern data were written in the PMMA resist using a Cambridge Instruments EBMF 10.5/CS electron beam lithography systemwith a 76-nm beam diameter and a 20 kV acceleration voltage. The two intermediate phases were obtained by use of square pillars of 350 nm and 550 nm on a side spaced 700 nm apart. The minimum phase level corresponded to complete exposure, while the maximum phase level corresponded to no exposure. The outer radii of the regions of constant phase are given by $r_m = ((f + ml/4)^2 - f^2)^{1/2}$. Following exposure, the PMMA was developed in 1:1 methyl isobutyl-ketone(MIBK) and isopropyl alcohol. The sample was then etched in a $BCl_3/Cl_2/CH_4$ plasma until the aluminum layer was cleared in the exposed areas. An oxygen ash converted remaining aluminum chloride residues into aluminum oxide to prevent corrosion of the aluminum mask upon exposure to atmospheric humidity.[11] A low-pressure, magnetically-confined CF_4 plasma was used to etch the fused quartz in the areas where the aluminum had been cleared. The etch was performed in steps, with the etch depth monitored by an Alpha-Step profilometer scan of an wide patch near the lens, until the desired etch depth was measured. Afterwards, the aluminum layer was removed with a 2:1

hydrochloric acid/nitric acid solution. The lens was sputter-coated with ~20 nm Au/Pd and examined with a scanning electron microscope. Figure 2a is a micro-graph of the lens. The four quadrants were stitched together without fine alignment with a common vertex at the center. The stitching errors were estimated to be 1 μm in the x-direction and 0.3 μm in the y-direction. These stitching errors are due primarily to the nonplanarity of the substrate. This is not expected to produce any degradation in the efficiency, since each quadrant has equal focusing power. However, the spot may suffer from slight aberrations due to the stitching. Figure 2b is a close-up of a section of one Fresnel zone.

The focusing power of the lens was characterized by a measurement of the first order diffraction efficiency. An efficiency of 53% was measured with a knife-edge at the focal plane and a detector. Due to scattering into higher orders, the use of a 700 nm period modulated grating generates amplitude modulation, which lowers the expected diffraction efficiency of the lens from 81% to 65%, in accordance with scalar diffraction theory. Additional calculations we have performed show that if a continuous phase variation from 0 to 2π is exploited, with a grating depth of 1.376 μm, the theoretical efficiency would easily surpass 80%. The subsequent feature dimension requirements, however, are difficult to achieve at the present time. The 12% measured discrepancy in efficiency arises from a combination of reasons. It is estimated that fabrication errors themselves contribute no more than 2% reduction. The breakdown of scalar theory, the breakdown of the homogenization approximation, and scattering from the transition ambiguity of the phase boundaries are the main sources of efficiency loss. In addition to efficiency, focal spot quality is an important measure of lens performance. A 20 X microscope objective was used to magnify the focal spot and an image of the spot was captured by a CCD camera system controlled by a microcomputer. Figure 3 is a picture of the point spread function, i.e., the intensity profile at the focal plane of the lens. The FWHM was measured to be ~15 μm, in agreement with the theoretical value, 1.22(F/#)l = 15.44 μm. The fact that the spot appears to lack symmetry may be attributed to field stitching in the electron beam

lithography, and may be eliminated if desired by use of alignment during lithography. Due to the small number of Fresnel zones, local surface imperfections and non-uniformities can be expected to have a more drastic effect on the spot profile.

The attractiveness of the MZOG design scheme we have presented in this Letter is the simplified fabrication process compared to multi-level or analog surface profiling techniques. Discrete, well-defined binary patterns are etched into fused quartz, an ideal substrate for most optical applications. The desired diffraction pattern is achieved through artificial index modulation rather than explicit surface-relief blazing. Electron-beam lithography was used for demonstration at a visible wavelength. Phase-shifting i-line (365 nm) lithography would enable feature sizes of 0.3 μm to be achieved, enabling demonstration at wavelengths of 1.3 μm and higher.[12] With the advent of KrF excimer laser (248 nm) lithography, the use of phase-shifting technology would push the resolution to 0.2 μm. These developments are encouraging for the mass production of diffractive micro-optical elements based on mostly-zeroth-order gratings.

References - section II

1. W. E. Kock, Bell Syst. Tech. J. **27**, 58 (1948).

2. W. Stork, N. Streibl, H. Haidner, and P. Kipfer, Opt. Lett. **16**, 1921 (1991).

3. M. W. Farn, Appl. Opt. **31**, 4453 (1992).

4. F. T. Chen and H. G. Craighead, Opt. Lett. **20**, 121 (1995).

5. P. Kipfer, M. Collischon, H. Haidner, and J. Schwider, Proc. SPIE **2169**, 100 (1994).

6. E. Noponen and J. Turunen, JOSA A **11**, 1097 (1994).

7. E. Noponen and J. Turunen, JOSA A **11**, 2494 (1994).

8. H. Dammann, Optik **31**, 95 (1970).

9. O. Joubert, G. S. Oehrlein, and Y. Zhang, J. Vac. Sci. Tech. A **12**, 658 (1994).

10. S. M. Shank, R. Soave, A. Then, and G. W. Tasker, J. Vac. Sci. Tech. B (in press).

11. S. M. Sze, *VLSI Technology*, McGraw-Hill, 1983, p. 226.

12. H. Watanabe and Y. Todokoro, J. Vac. Sci. Tech B **11**, 2669 (1993).

Figure Captions - section II

Figure 1: Efficiency and phase of transmitted zeroth order for a 700 nm period square pillar array as a function of pillar width. The pillar height is 1.032 μm and the wavelength used is 0.6328 μm. Only the component polarized parallel to the normally incident light is shown.

Figure 2a: Scanning electron micrograph of diffractive lens. The lens aperture is a 1 mm square and the focal length is 2 cm.

Figure 2b: Scanning electron micrograph of a section of one Fresnel zone, showing the four phase levels.

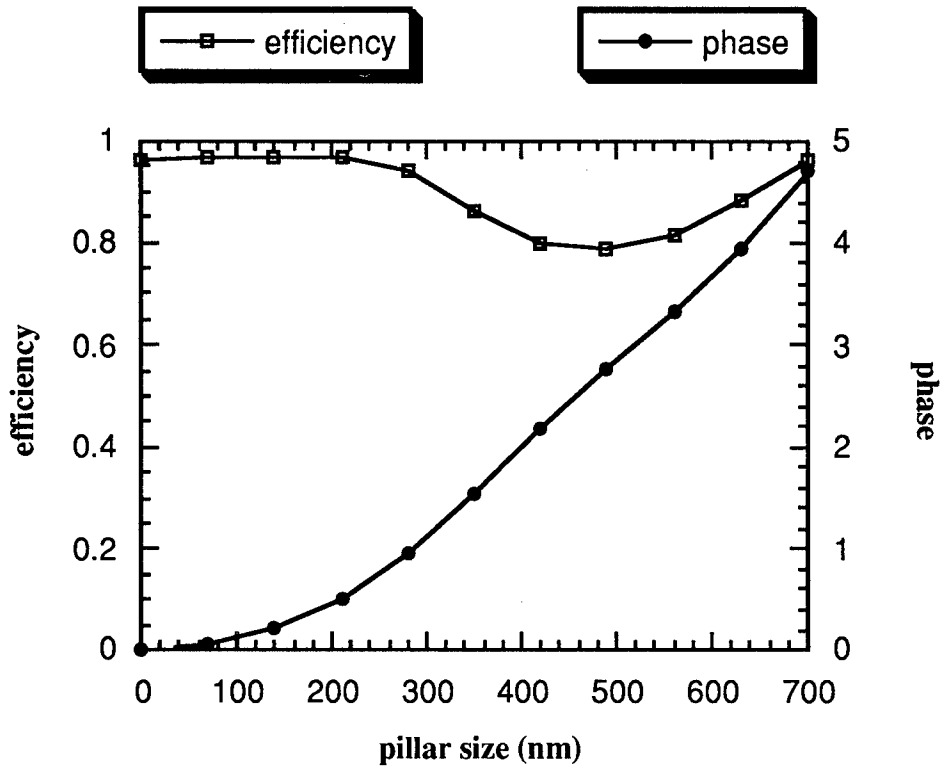Figure 3: Focal spot profile as measured by a CCD camera.
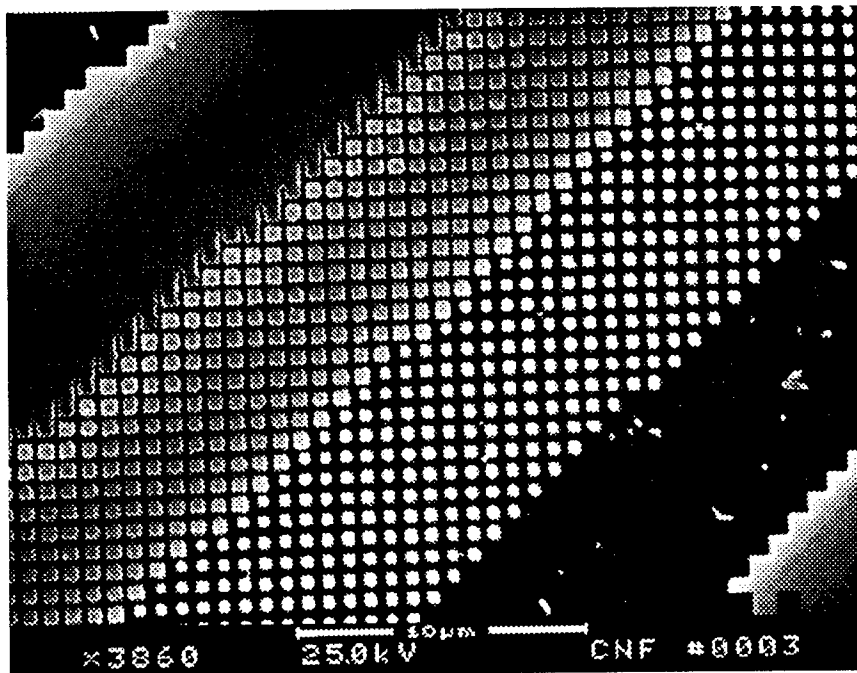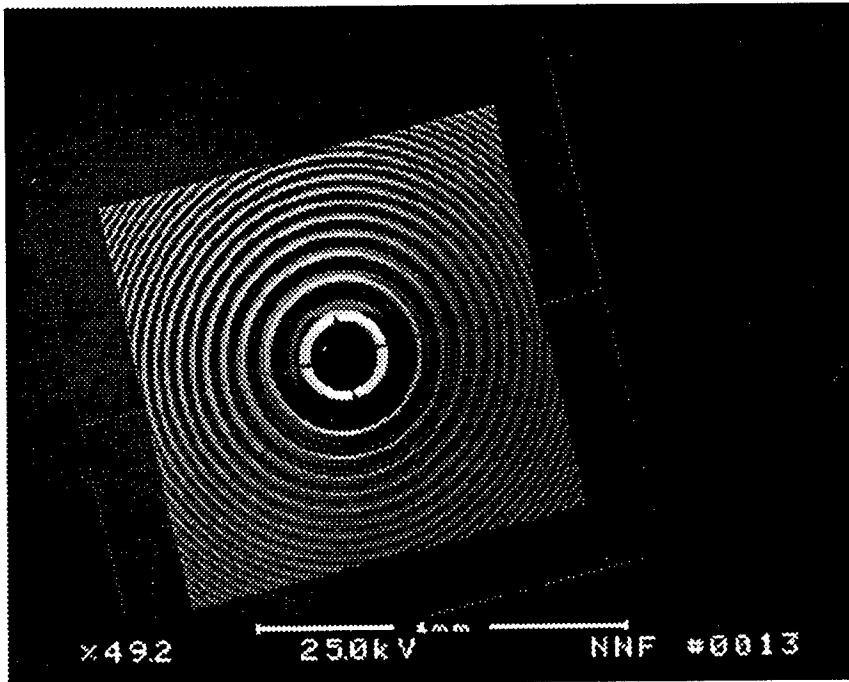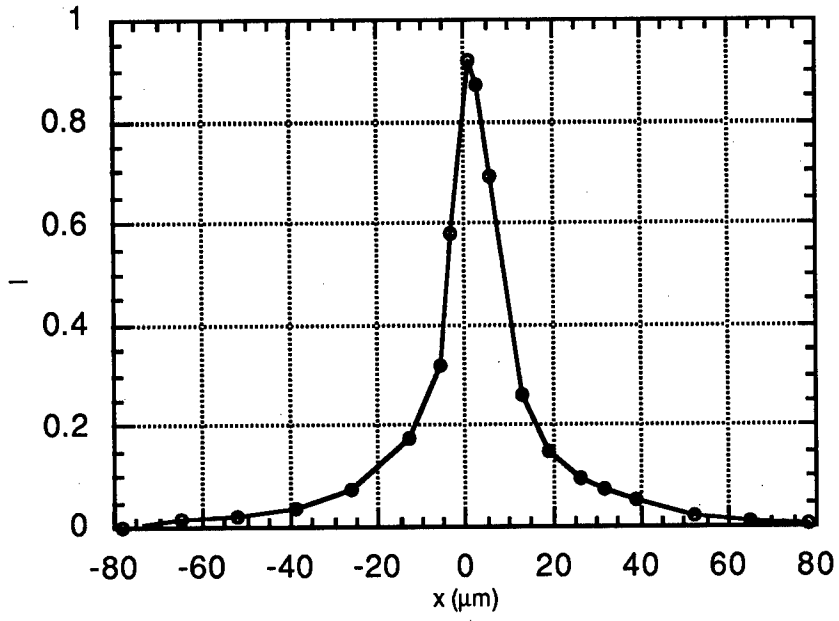
Figure II - 1

Figure II-2

Figure II-3

III. Black silicon as an antireflection coating

J. G. Couillard and H. G. Craighead

Silicon was etched using reactive ion etching with chlorine and flourine containing gasses. During etching, aluminum from the etch chamber was deposited onto the silicon surface, forming an *in situ* etch micromask. Etched surfaces were examined using scanning electron microscopy, and found to be contain columns of submicron width and height. The specular reflectance of these textured surfaces was measured for wavelengths of 300 to 1200 nm and found to have reflectances as low as 0.05% over the visible spectrum. These reflectances are more than 100 times less than those of an untreated silicon surface. Surfaces treated in this manner therefore have potential application as antireflection coatings in silicon-based optoelectronics. Theoretical calculations of the reflectance were performed, treating the textured layer as a uniform film with an index of refraction determined by effective media theory. Although the films are predicted by our calculations to reduce the reflectivity of the silicon surface, this theoretical treatment does not account for such a dramatic reduction in reflectivity.

Roughening of initially smooth silicon surfaces during reactive ion etching (RIE) is a frequent problem of semiconductor processing. Much has been written on the mechanism of this roughening, which is usually attributed to micromasking from the etch environment.[Oehrlein, 1986 #4; Oehrlein, 1990 #2; Thomas, 1989 #1] Non-volatile material formed in the etch plasma can deposit on the wafer surface and protect areas from the etch plasma. This random masking results in a rough surface. The composition of the micromask depends on the etch plasma. During Cl_2 RIE, water vapor in the etch chamber can form relatively stable SiO_x or $SiOH$ compounds on the silicon surface.[Thomas, 1989 #1] In fluorine-based plasmas aluminum removed from the chamber walls forms an equivalent mask material.[Oehrlein, 1986 #4]

The presence of micromasking is often detectable by the black appearance of the silicon surface after etching. This black appearance suggests that a micromasking technique might be used to create an anti-reflective coating on silicon. One advantage of such an approach is the ease with which the coating can be attained. No materials other than the initial silicon are required to produce the coating. Furthermore, the textured surface can have a low reflectivity over a wide band of wavelengths. Such an antireflection coating may prove useful in the development of silicon-based optoelectronics.

In order to use micromasking as an antireflection coating technique, a reliable etch process is needed. Micromasking during Cl_2 RIE, based on SiO_x or SiOH compounds, is dependent on water vapor in the etch chamber for formation of the mask. This technique appears unsuitable because humidity in the etch chamber may be difficult to control. Alternatively, CF_4 RIE relies on AlF_3 and related oxides as the micromask material. Since the aluminum is obtained from the etch chamber walls and electrodes the process is less dependent on outside conditions. AlF_3 makes a good micromask material because it is relatively nonvolatile. Unfortunately, this also makes it difficult to remove aluminum in the large quantities desired to produce uniform micromasking. One solution has been to use CCl_2F_2 as the etch gas.[Craighead, 1982 #3] The chlorine ions in the etch plasma are capable of forming volatile $AlCl_3$, which is then converted to more stable AlF_3 in the desired quantity. Since chlorofluorocarbons are currently restricted in their use, in this work we have developed a process using Cl_2 and CF_4 together in the etch plasma to achieve comparable results.

Experimental

Wafers of n-type Si were reactive ion etched in plasmas of Cl_2, CF_4, and O_2 over a wide range of flow rates (0-45 sccm), pressures (20-200 mtorr), and applied power (400-600 DC Volts). All etches used an aluminum plate as the anode. Samples with the lowest

reflectances were obtained by etching at 20 mtorr and 600 Volts DC bias with a plasma composed of 20, 10, and 45 sccm of Cl_2, CF_4, and O_2, respectively. SEM micrographs of etched samples show columnar structures on the surface of submicron diameter and spacing, with heights of 0.5 μm or more. An example is shown in figure 1.

Specular reflectance measurements of treated and untreated surfaces were collected using a CARY 5 UV-vis spectrometer in a modified "VW" configuration{ Strong, 1938 #7}. In this technique a measurement beam is reflected off of the sample surface at near-normal incidence (7°), and compared with a reference beam which has followed a similar path without undergoing a sample reflection. The wavelength range from 300 to 1200 nm was investigated. These measurements show dramatic reductions of the silicon reflectance for treated surfaces. (see figure 1) In samples processed under the conditions described above, the observed reflectance is less than 0.1% over the visible range of 300 - 900 nm.

Discussion

The spacing of the silicon columns on our micromasked surface is much less than the wavelengths of light used for our reflectance measurements. The surface may therefore be treated as an artificial dielectric film with a thickness equal to the height of the columns.{ Smith, 1979 #9; Kuester, 1990 #5} In such a film, the permittivity for an electric field perpendicular to the columns is approximately a combination of those of the substrate and the incident media,

$$\varepsilon_f \approx \frac{(1+f)\varepsilon_s + (1-f)\varepsilon_i}{(1-f)\varepsilon_s + (1+f)\varepsilon_i},$$

where f is the volume fraction of the film occupied by the substrate (Si).{ Hashin, 1962 #8; Kuester, 1990 #5}

The reflection from a transparent dielectric overlayer film of thickness d is:

$$R = \left| \frac{n_f(n_i - n_s)\cos(kn_f d) + i\left(n_s - n_f^2\right)\sin(kn_f d)}{n_f(n_i + n_s)\cos(kn_f d) + i\left(n_s + n_f^2\right)\sin(kn_f d)} \right|^2$$

where n_i, n_f, and n_s are the indices of refraction for the incident media, the overlayer film, and the substrate, respectively. k is the propagation number for the incident light in vacuum, $2\pi/l_0$.[Hecht, 1987 #6] We have extended this treatment to absorbing films. In an absorbing film, the reflectance becomes:

$$R = \left| \frac{n_f(n_i - n_s)\cosh\left[(\alpha + ikn_f)d\right] + \left(n_s - n_f^2\right)\sinh\left[(\alpha + ikn_f)d\right]}{n_f(n_i + n_s)\cosh\left[(\alpha + ikn_f)d\right] + \left(n_s + n_f^2\right)\sinh\left[(\alpha + ikn_f)d\right]} \right|^2$$

with a the absorption coefficient of the film.

We have used these formulas to estimate the index of refraction and reflection from a roughened silicon surface. The sample has a column height of aproximately 0.3 μm and a volume fraction of 0.37. According to our calculations, the reflectivity from this roughened silicon surface will be reduced by 30% on average from that of a bare silicon surface over the wavelength range 300 to 900 nm. The results of our calculations are shown in figure 2. However, this is not as dramatic a reduction as is seen experimentally (c.f. figure 1). It is reasonable to expect that Raleigh scattering of incident light from the roughened surface also plays a large role in reducing the specular reflection.

We have developed a reactive ion etch process for fabricating a columnar silicon surface, and explored the potential of such a film as an antireflection coating. Reflectance measurements show dramatically lower reflectivities for treated surfaces than untreated surfaces. The observed reflectances can be as low as 0.05% in the visible spectrum, or more than a 100-fold reduction in the reflectance of an untreated silicon surface. Application of effective media theories treating the roughened surfaces as effective dielectric films is insufficient to explain such a low reflectivity.

Figure Captions - section III

Figure 1 Measured reflectances of the roughened surface from figure 1, compared with that of an unetched silicon surface.

Figure 2 Calculated reflectances of both untreated and roughened silicon surfaces.
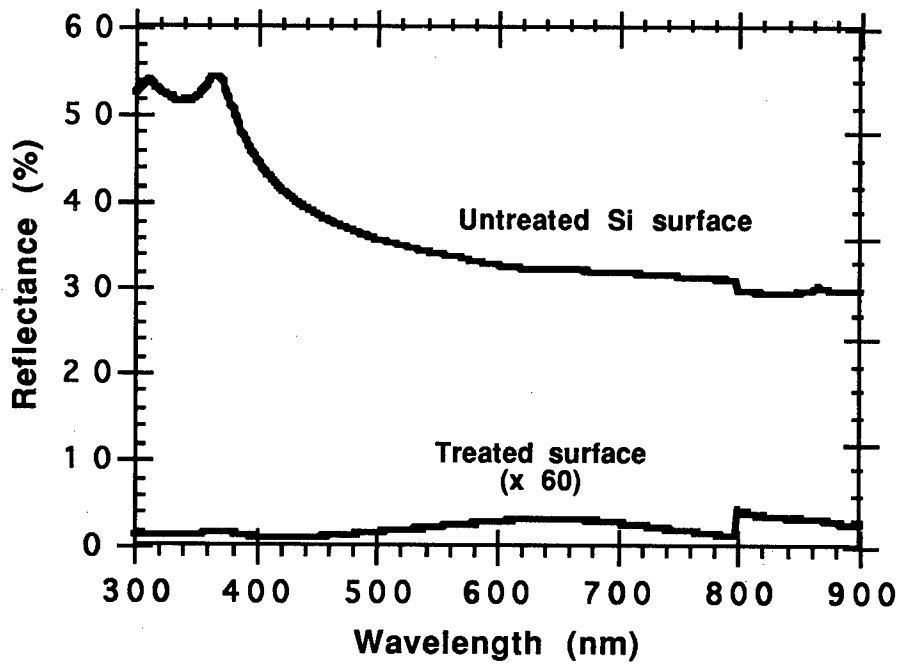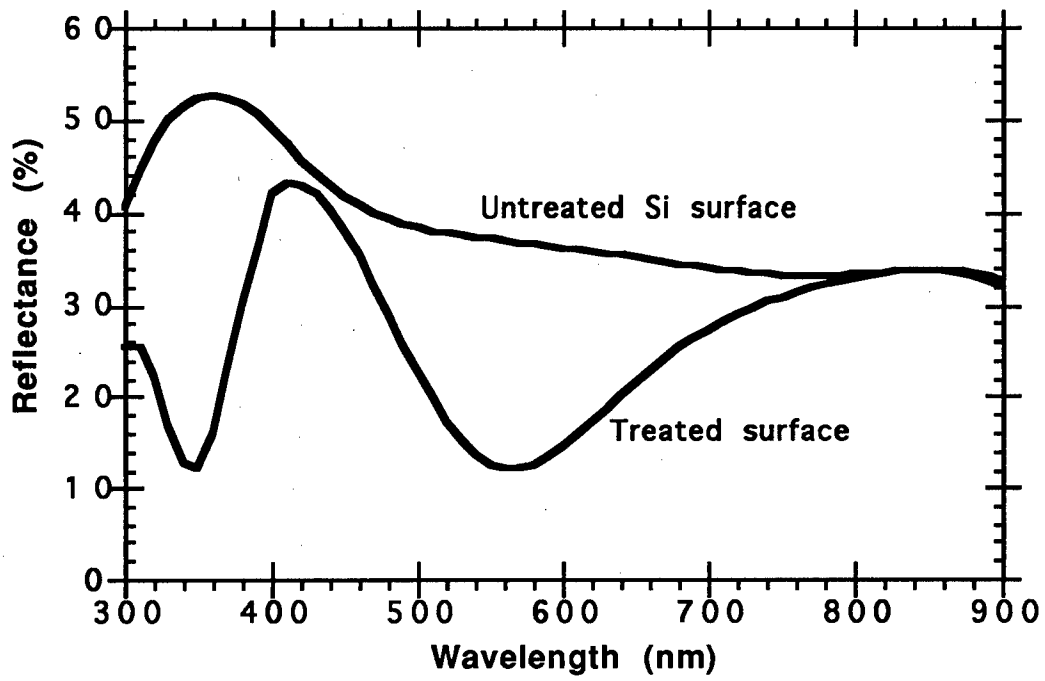
Figure III-1

Figure III - 2

MISSION

OF

ROME LABORATORY

Mission. The mission of Rome Laboratory is to advance the science and technologies of command, control, communications and intelligence and to transition them into systems to meet customer needs. To achieve this, Rome Lab:

    a. Conducts vigorous research, development and test programs in all applicable technologies;

    b. Transitions technology to current and future systems to improve operational capability, readiness, and supportability;

    c. Provides a full range of technical support to Air Force Materiel Command product centers and other Air Force organizations;

    d. Promotes transfer of technology to the private sector;

    e. Maintains leading edge technological expertise in the areas of surveillance, communications, command and control, intelligence, reliability science, electro-magnetic technology, photonics, signal processing, and computational science.

The thrust areas of technical competence include: Surveillance, Communications, Command and Control, Intelligence, Signal Processing, Computer Science and Technology, Electromagnetic Technology, Photonics and Reliability Sciences.